Shape Memory Alloy Actuator Integrated Morphing Aerofoil Structure

K. Dasharathi, A A Wadkar, A K Kancharla, D Roy Mahapatra*
Department of Aerospace Engineering, Indian Institute of Science, Bangalore, 560012, India Email: droymahapatra@aero.iisc.ernet.in

ABSTRACT

In this paper, we report new design and analysis of aerofoil morphing using Shape Memory Alloy (SMA) wire actuator. A finite element based computational model of the coupled SMA-aerofoil is developed incorporating the non-linear hysteretic deformation of the SMA wire actuator and low-speed aerodynamic pressure. This model is used for analysis of the preliminary aerofoil design. Simulation results from this model are reported. Based on these results, the aerofoil is redesigned and detailed analysis is carried out. Trailing edge deflection is optimized, and at the same time, it is ensured that the aerofoil is stiff enough for sustaining aerodynamic loads at velocities up to 20m/s. Experimental results obtained from a laboratory scale setup of SMA wire integrated aerofoil are reported and they are found to be in close agreement with the simulated results.

1. INTRODUCTION

Structural morphing involves altering the configuration of a structure in real time depending on the operating conditions to achieve optimized performance. Of late, the idea of developing aircraft structures that adapt to various operating conditions has attracted a tremendous amount of attention. Aircrafts with adaptive structural capabilities would have advantages such as expanded flight envelope and ability to carry out multiple missions i.e. reconnaissance, attack etc [1, 2]. As per Ref. [3], wing morphing is divided into three categories, namely (1) Large scale aircraft morphing – involves changing wing area, span and sweep; (2) Medium scale morphing – involves changing chord, camber, thickness, differential pitching angle and shape of individual aerofoil; (3) Small scale morphing – involves changes that affects local air flow (smart fin, flap and boundary layer control system). Our research is focused on medium scale morphing, i.e. changing the chord, camber and shape of the aerofoil to enhance the aerodynamic properties.

In the past various approaches have been adopted in attempts to successfully develop a morphing wing. A majority of these attempts originated from various large programs on flow circulation control system [4]. Among other approaches, using compliant mechanisms to achieve morphing is very popular [5-8]. Amprikidis et al. [6] have used a concept of "adaptive internal structures" to achieve morphing. Their concept involves altering the bending and torsional stiffness of the wings through changes in the internal aircraft structure. They rely on the aerodynamic forces to provide the moment to twist the wing. Ramrkahyani et al. [7] have employed compliant cellular truss made of SMAs with tendons as actuators for realizing morphing. Perkins et al. [8] have developed a morphing concept which involves sliding ribs covered with shape memory polymer (SMP) skin. While the methods involving compliant mechanisms do produce large displacement, they tend to cause aeroelastic problems such as flutter.

The other and more popular approach for wing morphing involves using smart materials such as shape memory alloys (SMAs), shape memory polymers (SMPs), piezo ceramic actuators, etc. Cadogan et al. [9] have employed piezoelectric actuators and pneumatic nastic structures on an inflatable wing to achieve morphing. They found that such an approach would require enormous forces for actuation which are not met by the piezo actuators. Since in piezoelectric actuators there is a trade-off between the amount of force generated and the deflection obtained, they are not suited for morphing applications. Vos et al. [10] have employed a new class of piezoelectric actuators known as post-

* Corresponding Author: Email: droymahapatra@aero.iisc.ernet.in; Tel: +91-80-22932419; Fax:+9180-23600134

buckled precompressed (PBP) actuators for morphing. They have replaced the conventional aileron part of the wing with a section made of this PBP actuator and have successfully demonstrated the roll control ability of this actuator on a sub-scale unmanned aerial vehicle (UAV). However the aerodynamic advantage and superior control that can be obtained by equipping the entire wing with morphing ability cannot be achieved by their design since their wing design would not be able to sustain high aerodynamic loads. SMAs on the other hand are light weight, produce large deformation and they have the highest energy density among the smart materials. This makes SMAs a very popular choice as actuators in wing morphing applications. Dong et al. [11] have employed SMA springs with axis positioned orthogonal to the chord and span directions to alter the shape of the aerofoil from one configuration to the other for optimizing the aerofoil contour depending on the flight conditions. Their approach requires only small deflection of the aerofoil skin and since it alters the local airflow, it comes under small scale morphing. Strelec et al. [12] have examined the feasibility of using SMA wires as linear actuators in designing a reconfigurable aerofoil to maximize lift-to-drag ratio. In order to have a continuous smooth change in aerofoil shape during morphing, they have used a genetic algorithm based design optimization technique to arrive at the optimal actuator configuration. They found that under subsonic flow conditions at angle of attack, the lift-to-drag ratio increased by 45% from the original unmorphed aerofoil.

However, one disadvantage of using the SMA wire actuators is that there is always a trade-off between the force that can be generated and the displacement that is obtained; this was confirmed by our preliminary experimental analysis on NACA0012 aerofoil. Thus, the approach we have adopted involves using a mechanism that is aided by SMA wire actuators for achieving aerofoil morphing. Another important fact is that the force generated by the SMA wire actuators may be inadequate to cause significant trailing edge deflection under the aerodynamic pressure. Since wing morphing is a complex phenomenon involving interaction between the air flow, the aerofoil structure and the SMA wire actuator, it is essential to study the effects of these on the deflection of the trailing edge. Therefore, to aid the design process, a model involving one-dimensional finite elements representing segments of the aerofoil and integrated with the SMA wire actuator is developed. In this model, the forces on the aerofoil due to aerodynamic pressure are incorporated. The aerodynamic pressure on the aerofoil is computed by source-vortex panel method under the assumption of a laminar incompressible inviscid flow field. The SMA wire actuator behavior is modeled using the one-dimensional phenomenological model reported in Ref. [13]. This model of SMA wire assumes various parameters describing the phase diagram for transformation as known quantities. The developed finite element model of the aerofoil integrated with SMA wire actuators is used for preliminary analysis of the ability of the SMA wire(s) to give trailing edge deflection under a flow field. During this analysis, various configurations of the SMA wire actuator are tested and the optimum configuration based on the trailing edge deflection is selected and implemented for experimental verification. In this paper, the results from the numerical and experimental analysis of the trailing edge deflection of a NACA0012 symmetrical aerofoil integrated with the SMA wire actuator are reported. Based on this preliminary analysis, design refinements are made. The new design involves a NACA4412 flat bottom aerofoil. In this, the stiffness of the upper skin is reduced using a polyurethane strip and the movement of the lower skin is enhanced using a slider mechanism. Theoretical analysis of such a complicated design is not straightforward using the developed finite element model of aerofoil segments with aerodynamic pressure as lumped and weakly coupled quantities. Hence a fully coupled fluid structure model is implemented using COMSOL/Multiphysics software. The results from the numerical and experimental analysis of the trailing edge deflection of the NACA4412 aerofoil are reported at the end of this paper. In summary, what is reported next in this paper is a significant and new development towards understanding various issues in fluid-structure-actuator coupling and the complexity of aerofoil morphing.

In section 2, the finite element model of the aerofoil integrated with the SMA wire actuator is reported. In sec. 3, the simulation and experimental results on the NACA0012 and NACA4412 modified aerofoil are reported.

2. FINITE ELEMENT MODEL OF SMA WIRE INTEGRATED AEROFOIL

The morphing strategy that we have adopted involves use of SMA wire actuator for deforming the aerofoil skin to give trailing edge deflection beside a small change in the camber. This model is developed for a preliminary analysis of the aerofoil integrated with the SMA wire. Using this model, various configurations of the SMA wire actuator are tested, and based on the trailing edge deflection a

sub-optimal configuration is selected for fabrication. These simulations are carried out under a flow field to determine the ability of the SMA wire to give adequate trailing edge deflection under aerodynamic pressure. The aerodynamic pressure on the aerofoil is computed by assuming laminar and incompressible flow. The aerofoil construction is such that the flexural deformation of the skin is absent at the leading and trailing edges. Therefore these parts of the aerofoil are considered rigid in the finite element model. The leading edge is fully restrained to avoid rigid body mode in finite element solution.

2.1 Model of the Aerofoil

A schematic diagram of the aerofoil integrated with the SMA wire actuator is shown in Fig. 1. The aerofoil skin is subjected to aerodynamic pressure distribution $P(x)$ and force due to SMA wire actuator. In this model, only the skin parts (region between X_1 and X_2 in Fig. 1) are considered as flexible. The leading and trailing edge stiffeners are taken as rigid bodies. Since the forces acting on the upper and the lower skins are not the same, the aerofoil is divided into regions *A* and *B* representing upper and lower skins, respectively. The SMA wire region is denoted by *S*. The deflections of the surfaces are obtained by solving the coupled differential equations for arbitrary curved segments, derived using Kirchhoff's kinematics.

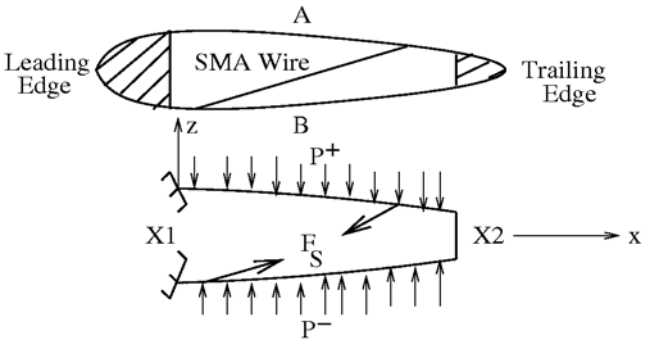

Figure 1. Schematic diagram showing the SMA wire and skin elements.

The thickness distribution for a NACA 4 digit aerofoil is given by

$$Z = \pm\frac{t}{0.2}(0.2969\sqrt{x} - 0.1260x - 0.3516x^2 + 0.2843x^3 - 0.1015x^4), \tag{1}$$

where t is the maximum thickness of the aerofoil and x is the chord axis. For modeling purpose, the wing is divided into a number of segments. Each segment is modeled as a plate strip with unidirectional bending. The displacement field (u, w) in the $x - y$ plane (aerofoil cross-sectional plane) is of Euler-Bernoulli beam type, that is,

$$u = u_0(x,t) - z\frac{\partial w}{\partial x}, \qquad w = w(x,t), \tag{2}$$

where u is the in-plane displacement measured with respect to the segment-local coordinate, u_0 is the in-plane displacement of the neutral plane, z is the thickness coordinate measured with respect to the neutral plane of the current segment, $z\partial w/\partial x$ is the in-plane displacement due to bending and w is the transverse displacement. Using Hamilton's first principle, the governing equations for the in-plane motion and the out-of-plane motion are obtained as

$$\delta u_0: \quad \rho A_0 u_0 - EA_0\frac{\partial^2 u_0}{\partial x^2} + EA_1\frac{\partial^3 w}{\partial x^3} - \rho A_1\frac{\partial w}{\partial x} + f_u = 0, \tag{3}$$

$$\delta w: \quad \rho A_0 w - EA_1\frac{\partial^3 u_0}{\partial x^3} + EI\frac{\partial^4 w}{\partial x^4} + \rho A_1\frac{\partial u_0}{\partial x} - \rho I\frac{\partial^2 w}{\partial x^2} + f_w = 0, \tag{4}$$

where f_u and f_w denote the distributed forces per unit length acting throughout the aerofoil surface in the in-plane and transverse directions, respectively. Neglecting the inertia terms for this problem, the governing differential equations for the upper and lower skins are expressed as

$$EA_0 \frac{\partial^2 u_{0_A}(x)}{\partial x^2} - EA_1 \frac{\partial^3 w_A(x)}{\partial x^3} = f_{u_A}, \tag{5}$$

$$EA_0 \frac{\partial^4 w_A(x)}{\partial x^4} - EA_1 \frac{\partial^3 u_{0_A}(x)}{\partial x^3} = -P^+, \tag{6}$$

$$EA_0 \frac{\partial^2 u_{0_B}(x)}{\partial x^2} - EA_1 \frac{\partial^3 w_B(x)}{\partial x^3} = f_{u_B}, \tag{7}$$

$$EA_0 \frac{\partial^4 w_B(x)}{\partial x^4} - EA_1 \frac{\partial^3 u_{0_B}(x)}{\partial x^3} = -P^-, \tag{8}$$

where the subscripts A and B denote the quantities associated with the upper and lower skins, respectively. The cross-sectional constants are $A_0 = bh$, $A_1 = bh^2/4$, $I = bh^3/12$, where E is the young's modulus, h is the thickness of the aerofoil skin, b is the span of the aerofoil, f_{u_A} and f_{u_B} denote the in-plane forces per unit length (due to skin friction), P^+ and P^+ are the z component of the aerodynamic pressures acting on the upper and lower skins, respectively.

2.2 SMA Wire Model

In this finite element model, the SMA wires are considered to be placed at an angle o with respect to the Z axis (see Fig. 1). In order to describe the SMA wire behavior, the constitutive law proposed by Brinson [13] is used; which is given by

$$\sigma - \sigma_0 = D(\xi)\varepsilon - D(\xi_0)\varepsilon_0 - \varepsilon_l D(\xi)\xi_s + \varepsilon_l D(\xi_0)\xi_{S0} + \Theta(T - T_0), \tag{9}$$

where θ is the stress in the SMA wire, θ_0 is the bias stress, $D(\xi)$ is the elastic modulus of the wire, ϖ is the martensite volume fraction, χ_0 is the initial strain in the wire, χ_l is the maximum recoverable strain, O is the thermal stress coefficient, T is the temperature of the wire and T_0 is the initial temperature of the wire. The modulus of elasticity $D(\xi) = D_a + (D_m - D_a)\xi$, where D_a is the modulus of elasticity of the austenite phase and D_m is the modulus of elasticity of the martensite phase. The martensite volume fraction $\xi = \xi_S + \xi_T$, where ϖ_S is the stress induced martensite and ϖ_T is the temperature induced martensite. The momentum balance equation for the SMA wire can be written as

$$\frac{\partial \sigma(\xi, T, \varepsilon)}{dz'} = \frac{\partial}{\partial z'}\Big[\Big(D(\xi)\varepsilon - D(\xi_0)\varepsilon_0 - \varepsilon_l D(\xi)\xi_S + \varepsilon_l D(\xi_0)\xi_{S0} + \Theta(T - T_0)\Big)\Big] = 0, \tag{10}$$

with the boundary conditions $\sigma A_{SMA} = \pm F_S$, where A_{SMA} is the cross-sectional area of the SMA wire, F_S is the force developed in the SMA wire (see Fig. 1) and $z' = L - g(u, w)$ represents the instantaneous length of the SMA wire due to some function g of the deflections (u, w) of the upper and lower skins.

The finite element model of the SMA wire integrated aerofoil is derived by coupling the governing equations of the aerofoil skin segments and the SMA wire. The weak solution for the system of coupled nonlinear partial differential equations. (5)-(8) and (10) is obtained by minimizing the weighted residual form as

$$\begin{aligned}
&\int \delta\overline{u}_A[EA_0 \frac{\partial^2 u_{0_A}(x)}{\partial x^2} - EA_1 \frac{\partial^3 w_A(x)}{\partial x^3} - f_{u_A}]dS_A + \int \delta\overline{w}_A[EI \frac{\partial^4 w_A(x)}{\partial x^4} - EA_1 \frac{\partial^3 u_{0_A}(x)}{\partial x^3} + P^+]dS_A \\
&+\int \delta\overline{u}_B[EA_0 \frac{\partial^2 u_{0_B}(x)}{\partial x^2} - EA_1 \frac{\partial^3 w_B(x)}{\partial x^3} - f_{u_B}]dS_B + \int \delta\overline{w}_B[EI \frac{\partial^4 w_B(x)}{\partial x^4} - EA_1 \frac{\partial^3 u_{0_B}(x)}{\partial x^3} + P^+]dS_B \\
&+\int \delta\overline{u}_S[\frac{\partial \sigma(\xi, T, \varepsilon)}{\partial z'}]d\Omega_E = 0,
\end{aligned} \tag{11}$$

where $dS_A = \sqrt{1 + (dZ_A / dx)^2}\,dx = \lambda_A dx,\ dS_B = \sqrt{1 + (dZ_B / dx)^2}\,dx = \lambda_B dx,$, $\mathbf{Y}_E$ denotes the volume of the SMA wire, the quantities with overhead bar $(\overline{u}_A, \overline{w}_A, \overline{u}_B, \overline{w}_B, \overline{u}_S)$ are the weight functions from the

space of admissible functions which minimizes the total energy of the system. Z_A and Z_B denote the coordinate of the aerofoil given in Eq. (1). The subscripts *A, B* and *S* denote the quantities related to the upper surface, lower surface and the SMA wire in its local coordinate, respectively. Implementing suitable interpolation functions for in-plane and out-of-plane displacements, and integrating Eq. (11) by parts, we get the finite element system equation, which can be written in the matrix-vector form as

$$\begin{bmatrix} [K]_{AA} & [K]_{AB} & [K]_{AS} \\ [K]_{BA} & [K]_{BB} & [K]_{BS} \\ [K]_{SA} & [K]_{SB} & [K]_{SS} \end{bmatrix} \{u\}^e = \{F\}^e, \tag{12}$$

where $\{u\}^e = \{\{\ u_A \quad w_A\ \}\{\ u_B \quad w_B\ \}\{\ u_S \quad w_S\ \}\}^T$ denotes the nodal displacement vector and $\{F\}^e = \{\{F_A\}\{F_B\}\{F_S\}\}^T$ denotes the nodal force vector. The elements of the stiffness matrix are obtained as

$$K_{AA} = -\int N_u^T EA_0 D_u \lambda_A' \, dx - \int D_u^T EA_0 D_u \lambda_A' \, dx + \int N_u^T EA_1 B_w \lambda_A' \, dx + \int D_u^T EA_1 B_w \lambda_A \, dx + 2\int D_w^T EIB_w \lambda_A' \, dx$$
$$+ \int N_w^T EIB_w \lambda_A'' \, dx + \int B_w^T EIB_w \lambda_A \, dx - 2\int D_w^T EA_1 D_u \lambda_A' \, dx - \int N_w^T EA_1 D_u \lambda_A'' \, dx - \int B_w^T EA_1 D_u \lambda_A \, dx,$$

$$K_{BB} = -\int N_u^T EA_0 D_u \lambda_B' \, dx - \int D_u^T EA_0 D_u \lambda_B' \, dx + \int N_u^T EA_1 B_w \lambda_B' \, dx + \int D_u^T EA_1 B_w \lambda_B \, dx + 2\int D_w^T EIB_w \lambda_B' \, dx$$
$$+ \int N_w^T EIB_w \lambda_B'' \, dx + \int B_w^T EIB_w \lambda_B \, dx - 2\int D_w^T EA_1 D_u \lambda_B' \, dx - \int N_w^T EA_1 D_u \lambda_B'' \, dx - \int B_w^T EA_1 D_u \lambda_B \, dx,$$

where

$$\lambda' = \frac{\partial \lambda}{\partial x}, \qquad \lambda'' = \frac{\partial^2 \lambda}{\partial x^2},$$

$$[K]_{AB} = [K]_{BA}, \qquad [K]_{AS} = [K]_{BS} = [K]_{SA} = [K]_{SB} = 0,$$

$$[K]_{SS} = [\Gamma]^T [K']_{SS} [\Gamma], \qquad [K']_{SS} = \int D_u^T D(\xi) D_u \, dz,$$

$$[\Gamma] = \begin{bmatrix} \cos\theta & \sin\theta & 0 & 0 \\ -\sin\theta & \cos\theta & 0 & 0 \\ 0 & 0 & \cos\theta & \sin\theta \\ 0 & 0 & -\sin\theta & \cos\theta \end{bmatrix},$$

where *o* is the angle with respect to Z-axis at which the SMA wire is placed within the aerofoil. The element of the force vectors due to aerodynamic pressure and the SMA wire are obtained as

$$\{F\}_A = \int N_w^T P^+ \lambda \, dx, \qquad \{F\}_B = \int N_w^T P^- \lambda \, dx, \qquad \{F\}_S = [\Gamma]^T F_S',$$

$$F_S' = \int D_u^T [\sigma_0 - D(\xi_0)\varepsilon_0 - \varepsilon_l D(\xi)\xi_S + \varepsilon_l D(\xi_0)\xi_{S0} + \Theta(T - T_0)] \, dz,$$

where $\{F_A\}$ and $\{F_B\}$ denote the forces acting on the aerofoil due to aerodynamic pressure distribution and $\{F_S\}$ denotes the forces exerted by the SMA wire. This force $\{F_S\}$ varies with the temperature of the SMA wire, which in turn changes $\{F_A\}$ and $\{F_B\}$ as the aerofoil coordinates are updated at each step of actuation of the SMA wire by thermo-electric heating.

2.3 Aerodynamic Pressure Distribution

The flow over the aerofoil skins is assumed to be laminar, incompressible, inviscid and steady. Assumption of steady flow requires that the thermo-electric actuation is very slow. The aerodynamic pressure is computed using a two-dimensional source-vortex panel method. The aerofoil is considered to be placed in a flow field with a uniform velocity U. The velocity potential due to the uniform flow is super-imposed on the velocity potential due to the disturbed flow around the aerofoil to obtain the total velocity potential, which is given by

$$\Phi = Ux + \phi, \tag{13}$$

where Ux is the free-stream potential and δ is the disturbance potential. The continuity condition for an incompressible flow, $\nabla \cdot U = 0,$ becomes a Laplace equation for the potential Δ, which is given by

$$\nabla \cdot (\nabla \Phi) = 0. \tag{14}$$

The disturbance potential δ around the aerofoil can be modeled by a distribution of sources and vortices over the surface. Kutta condition is satisfied by using the condition that the magnitude of velocities on the upper and the lower surfaces approach the same limiting value as the trailing edge is approached. The aerofoil surface is discretized into N number of panels and the sources and vortices of uniform strength per unit length are assumed to be acting over each of them. The sources and vortices distributed over a panel j induce a velocity $\overline{V_{ij}}$ at the collocation point of the panel i. The normal velocity V_{ni} and the tangential velocity V_{ti} at the collocation point are given by

$$V_{ni} = \sum_{j=1}^{N} \overline{p}_j \overline{N}_{ij} + \gamma \overline{N}_{i,N+1} + U \cdot \hat{n}_i, \tag{15}$$

$$V_{ti} = \sum_{j=1}^{N} \overline{p}_j \overline{t}_{ij} + \gamma \overline{t}_{i,N+1} + U \cdot \hat{t}_i, \tag{16}$$

where $\hat{n}_i$ and $\hat{t}_i$ are the unit normal and tangential vectors respectively. $\overline{N}_{ij}$ and $\overline{t}_{ij}$ are the normal and tangential influence coefficients respectively. $\overline{p}$ denotes the source strength per unit contour and ε denotes the vortex strength per unit length. Sine the surface represented by the panel is a solid surface, the surface normal velocity of the fluid at each collocation point must be either zero or prescribed to be the normal velocities obtained from the previous solution step. This condition gives N equations, which are supplemented by the Kutta condition giving a total of $N + 1$ equations. The Kutta condition can be written mathematically by equating the magnitude of the tangential velocities at the collocation points of the two panels defining the trailing edge as

$$\sum_{j=1}^{N} \overline{p}_j \overline{t}_{r,j} + \gamma \overline{t}_{r,N+1} + U \cdot \hat{t}_r = -\left(\sum_{j=1}^{N} \overline{p}_j \overline{t}_{r+1,j} + \gamma \overline{t}_{r+1,N+1} + U \cdot \hat{t}_{r+1} \right). \tag{17}$$

Here the subscripts r and $r + 1$ denote the panels connecting the trailing edge. By solving Eq. (14) with the help of Eqs. (15)-(17) at the collocation points, we get 'N' number of source strength per unit length and vortex strengths per unit length. The tangential velocities are obtained from Eq. (16) at each panel. The pressure at each collocation point i is calculated with the help of the Bernoulli equation. The coefficient of pressure at the i^{th} collocation point is obtained as

$$C_{pi} = 1 - \left(\frac{V_{ti}}{U} \right)^2. \tag{18}$$

Distribution of coefficient of pressure is obtained using Eq. (18) and it is used in determining the coefficient of lift. This finite element model of SMA wire integrated aerofoil has been implemented in MATLAB. The iterative solution procedure of this finite element model coupled with the 2D panel code is schematically illustrated in Fig. 2.

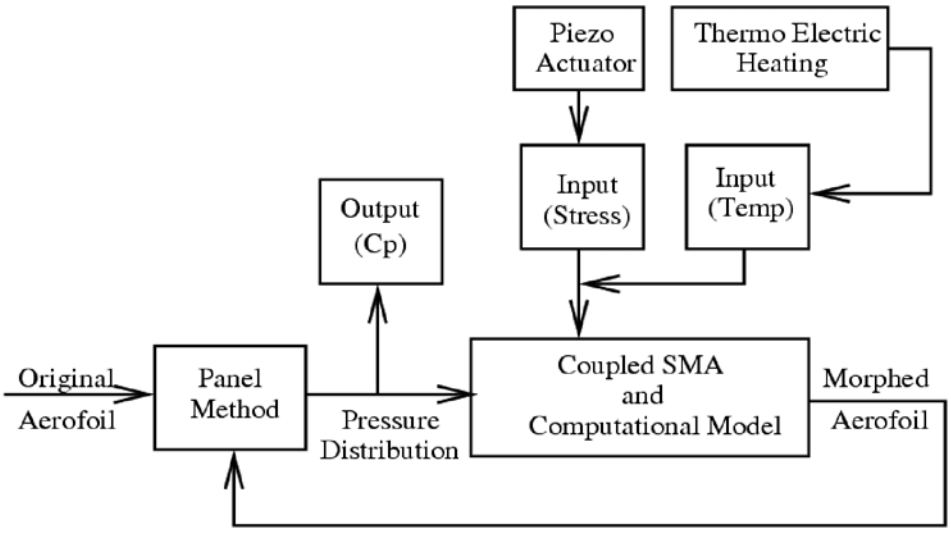

Figure 2. The solution scheme adopted for the developed finite element model.

3. SIMULATION AND EXPERIMENTAL RESULTS

The design strategy we adopt primarily involves a four step iterative procedure. In the first step, the finite element model developed above is used to analyze a basic aerofoil design. These analyses involve testing of various configurations of the SMA wire and select the best configuration depending on the maximum trailing edge deflection with sub-optimal stiffness. The second step involves fabrication and testing of this sub-optimal configuration. In the third step, based on the experimental results, the aerofoil is redesigned. This process of redesigning is an iterative process involving a detailed design study, done in a multiphysics simulation environment for complicated designs, to arrive at the optimum configuration. The fourth step involves fabrication and testing of this optimum configuration.

3.1 Design and Analysis of NACA0012 Aerofoil

In order to develop a morphing wing, a NACA0012 symmetric aerofoil made of aluminum, having a chord length 30cm and skin thickness 1mm is considered. Stress induced transformation of the SMA wire is chosen as the actuation means. The properties of the SMA wire are given in Table 1. During the preliminary design study of NACA0012 aerofoil, the developed finite element model is used to test various configurations of the SMA wire integrated aerofoil. These tests are done under the following conditions: angle of attack of , flow velocity of 20m/s, temperature of the SMA wire is maintained constant at for stress-induced (super-elastic) actuation for a wire diameter of 0.5mm. The results indicate that very high stress levels (in excess of 500MPa) are required to get trailing edge deflection of about 1cm (see Fig. 3). For experimental realization of this, powerful piezo stack actuators may be used to generate such high stress levels in the SMA wire. Conventional linear drives or stepper motors may be considered, although this would make the aerofoil very bulky and impractical for UAV applications. Therefore, the idea of using stress-induced transformation of the SMA wire as the actuation means is not pursued further in the following discussion.

Following this, several configurations of SMA wire integrated with the NACA0012 aerofoil are tested for thermal actuation of the SMA wire. The best aerofoil configuration is determined and fabricated. This configuration is tested experimentally using thermo-electric actuation of the SMA wire. The properties of the SMA wire used in simulations and experiments of temperature induced actuation are given in Table 2. The schematic diagram of the experimental setup is shown in Fig. 4 and the actual experimental setup of NACA0012 aerofoil is shown in Fig. 5. In the thermo-electric actuation of the SMA wire, the temperature of the SMA wire is regulated by controlling the electric current through the

SMA wire. In these morphing experiments, the temperature of the SMA wire is restricted below. For this, the electric current passed through the SMA wire is in the range of 0-2.5A. A higher temperature than what is normally expected is required here for full transformation, which is because of stress built up due to structural stiffness of the aerofoil. The ambient temperature is maintained at . The temperature of the SMA wire is measured using a K type thermo-couple and the trailing edge deflection is measured using a laser displacement sensor. The morphing experiments are carried in a quasi-static manner. Also there is no flow over the aerofoil, i.e., the aerodynamic loads on the aerofoil are absent in the laboratory scale setup. Fig. 6(a) shows the variation in the voltage applied and Fig. 6(b) shows the trailing edge deflection of NACA0012 aerofoil. It is observed that the trailing edge deflection of the aerofoil is about 2.3mm, which corresponds to about of trailing edge rotation. This is largely insufficient for actual UAV application and therefore calls for a modification in the design. During this experiment, it is observed that during downward deflection of the trailing edge, the upper skin is under a flexural load and the bottom skin is under a shear load. It is also observed that the stiff aluminum skin of the aerofoil offers great resistance to the deflection of trailing edge. Also, the stress levels achieved through thermo-electric actuation of SMA wire are not very high. Thus, to achieve sufficient trailing edge deflection, the aerofoil needs to be modified and a better mechanism must be devised so that the upper skin moves freely in bending and the lower skin in shear.

Table 1. Properties of the SMA wire used in stress induced actuation simulations.

Elastic Modulus, Density	Transformation Temperatures	Transformation Constants	Other Constants
$D_a = 67\times10^3$ MPa	$M_f = 9^\circ$C	$C_M = 8$MPa/ C	$\varepsilon_l = 0.067$
$D_m = 26.3\times10^3$ MPa	$M_s = 18.4^\circ$C	$C_M = 13.8$MPa/ C	$d = 0.5\times10^{-3}$ m
$\Theta = 0.55$MPa/$^\circ$C	$A_s = 34.5^\circ$C	$\sigma_s^{cr} = 100$MPa	$L = 0.189$m
	$A_f = 49^\circ$C	$\sigma_f^{cr} = 170$MPa	$T_{amb} = 24^\circ$C

Table 2. Properties of the SMA wire used in simulation and experiment, considering thermal actuation.

Elastic Modulus, Density	Transformation Temperatures	Transformation Constants	Other Constants
$D_a = 63\times10^3$ MPa	$M_f = 38^\circ$C	$C_M = 0.9$MPa/ C	$\varepsilon_l = 0.04$
$D_m = 30\times10^3$ MPa	$M_s = 46^\circ$C	$C_M = 0.9$MPa/ C	$d = 0.5\times10^{-3}$ m
$\Theta = 0.55$MPa/$^\circ$C	$A_s = 58^\circ$C	$\sigma_s^{cr} = 0$MPa	$L = 0.159$m
	$A_f = 68^\circ$C	$\sigma_f^{cr} = 50$MPa	$T_{amb} = 24^\circ$C

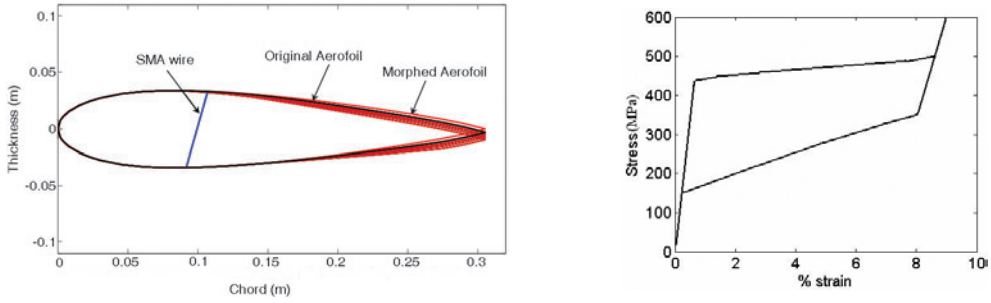

(a) (b)

Figure 3. (a) NACA0012 original and morphed aerofoil using stress induced transformation of SMA wire (b) hysteretic behavior of the SMA wire during morphing.

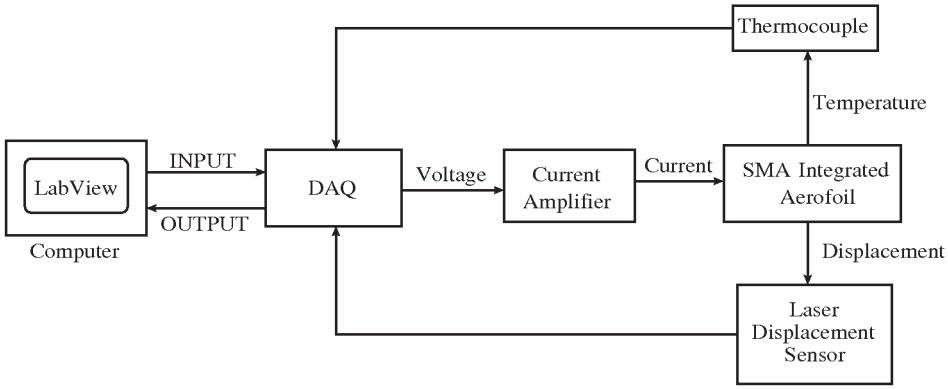

Figure 4. Schematic of the experimental setup used for the morphing of aerofoil.

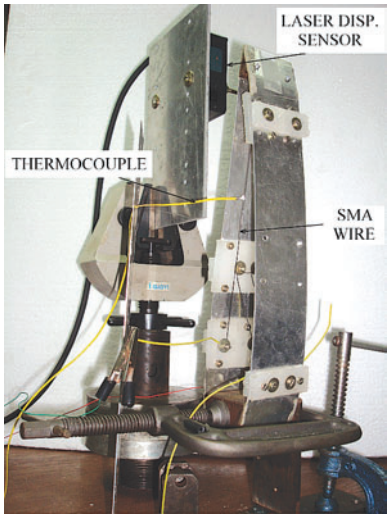

Figure 5. Experimental setup of NACA0012 aerofoil.

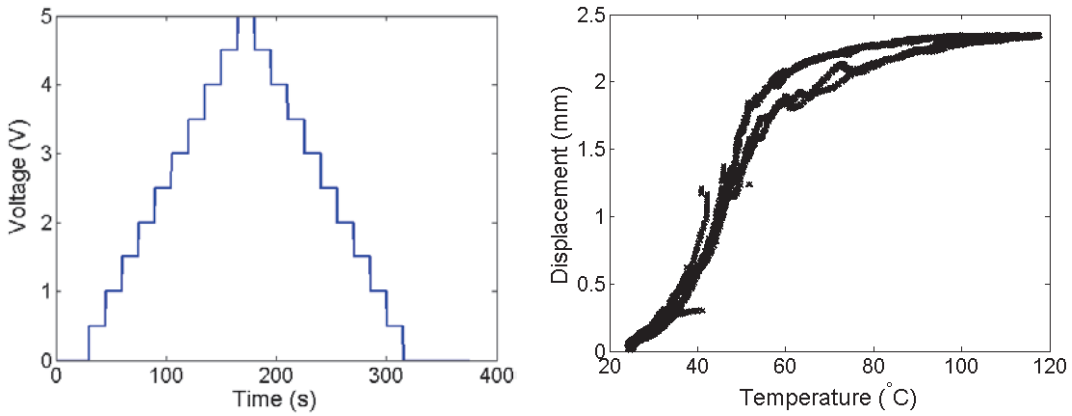

(a) (b)

Figure 6. (a) Variation in applied voltage (b) Trailing edge deflection of NACA0012 aerofoil.

3.2 Design and Analysis of NACA4421 Modified Aerofoil

The experimental results obtained from the NACA0012 aerofoil form the basis for design modification. The symmetric NACA0012 aerofoil does not allow easy movement of the lower skin in shear. Therefore NACA4421 aerofoil is selected for modification by integrating the SMA wires. Preliminary analysis of this aerofoil is carried out using the developed finite element model. In these preliminary simulations, un-modified NACA4421 aerofoil, i.e., aerofoil without any mechanisms is considered. The chord length of the aerofoil is taken as 30cm and the thickness of the aerofoil skin is 1mm. Various configurations of the SMA wire are tested considering that the aerofoil is at an angle of attack of and the flow velocity is 20m/s. The SMA wire properties for these simulations are given in Table 2. The SMA wire is considered to be under an initial stress of 50MPa. The simulation results indicate a trailing edge deflection of 2.7mm. The un-morphed and morphed aerofoil shapes are shown in Fig. 7. The point 'A' represents the trailing edge position of the un-morphed aerofoil and 'B' represents the trailing edge location after morphing.

A trailing edge deflection of 2.7mm is still insufficient. Therefore, to maximize the trailing edge deflection further, another design alteration has been conceived. This altered design consists of a slider mechanism on the lower skin to facilitate easy displacement under a shear load and a polyurethane strip on the upper skin to reduce the bending stiffness. The slider mechanism emulates a ball bearing mechanism and the lower skin of the aerofoil, slides between the two races of steel balls. This mechanism is shown in Fig. 8. A small portion of the upper skin, about 2cm in width, is cut at approximately 70% of chord length and is replaced using a polyurethane strip. Where as, the slider mechanism is attached on the lower skin. To obtain maximum trailing edge deflection from the redesigned aerofoil, it is essential to optimize the location of the slider. Simulation and analysis of such complicated design is beyond the scope of the developed finite element model of aerofoil segments with lumped aerodynamic load. Thus, a fully coupled analysis of this redesigned aerofoil is done using a multiphysics software COMSOL. In this analysis however, the SMA wire is not modeled in COMSOL to avoid complication due to hysteretic motion, and instead it is represented using an equivalent force hysteresis at the corresponding nodal points.

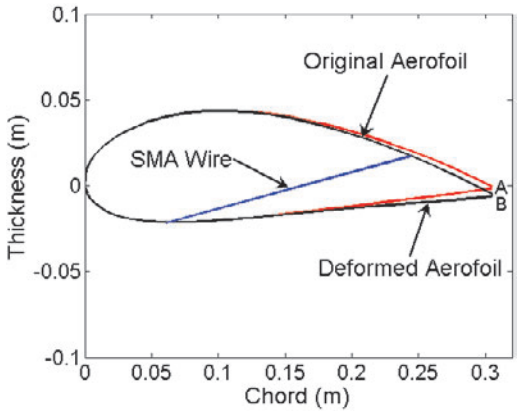

Figure 7. A Comparison of deformed and un-deformed shape of NACA4421 un-modified aerofoil obtained from the finite element simulation.

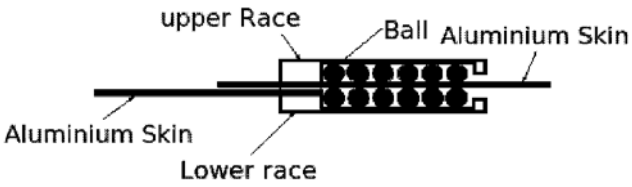

Figure 8. Schematic of the slider mechanism employed on the lower skin of aerofoil.

In this coupled fluid-structure-actuator model, the aerofoil is represented in two dimensions ($x - y$ plane), i.e. the span-wise length of the wing strip has not been modeled. The dynamic nature of loading

is also not incorporated. The solution of this model is obtained using finite element discretization and UMFPACK direct solver. The geometry of the aerofoil skin is discretized using triangular elements. The discretized model consists of 2302 elements. The solution of this model is obtained using plane-strain approximation in the plane elasticity equations of motion. The two-dimensional plane elasticity equations of motion are given by

$$\rho \frac{\partial^2 u_x}{\partial t^2} - \frac{\partial \sigma_{xx}}{\partial x} - \frac{\partial \sigma_{xy}}{\partial y} - f_x = 0, \tag{19}$$

$$\rho \frac{\partial^2 u_y}{\partial t^2} - \frac{\partial \sigma_{xy}}{\partial x} - \frac{\partial \sigma_{yy}}{\partial y} - f_y = 0, \tag{20}$$

where u_x and u_y represents the displacement in x and y directions, θ_{xy} is the shear stress, θ_{xx} and θ_{yy} are normal stresses. In the plane strain approximation,

$$\varepsilon_{xz} = \varepsilon_{yz} = \varepsilon_{zz} = 0, \tag{21}$$

$$\varepsilon_{xx} = \frac{\partial u_x}{\partial x}, \qquad 2\varepsilon_{xy} = \frac{\partial u_x}{\partial y} + \frac{\partial u_y}{\partial x}, \qquad \varepsilon_{yy} = \frac{\partial u_y}{\partial y}. \tag{22}$$

Simulations are carried out by considering three different locations of the slider mechanism. They are at 60%, 65% and 70% of the chord length, measured from leading edge, respectively. The location of the polyurethane strip is maintained at 70% of the chord length. The original shape and the deformed shape of the aerofoil for each of these cases are shown in Figs. 9-11. The trailing edge displacement observed for the 60%, 65% and 70% locations of the slider are 6.22, 3.49 and 1.69mm, respectively. From these results it is observed that as the slider mechanism is moved towards to leading edge, the stiffness of the aerofoil decreases and more trailing edge deflection is observed. It is important to note that if the stiffness of the aerofoil decreases too much, then the pre-stress in the SMA wire would also decrease. If the stress in the SMA wire decreases, there would not be complete recovery of the SMA wire deformation. Here "recovery" means recovery of the aerofoil shape from the bent position back to original position. Therefore, in the experimental aerofoil, the slider mechanism is attached at the location corresponding to 65% chord length.

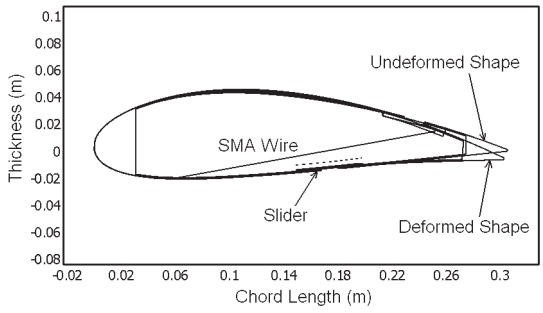

Figure 9. Deformed and un-deformed aerofoil for slider at 60% location of chord.

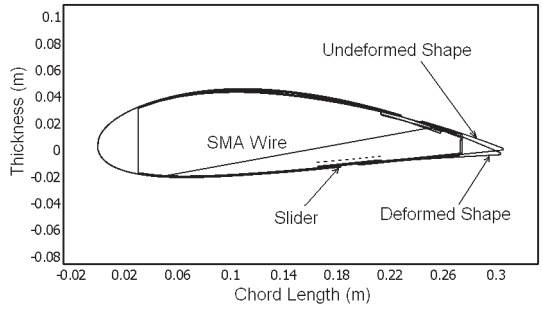

Figure 10. Deformed and un-deformed aerofoil for slider at 65% location of chord.

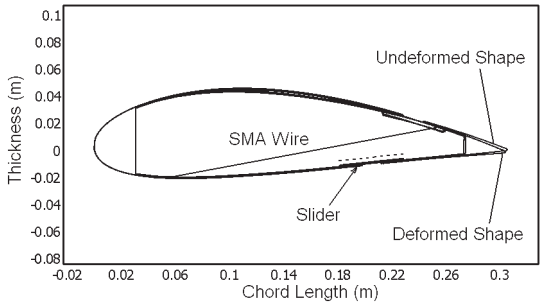

Figure 11. Deformed and un-deformed aerofoil for the slider at 70% location of chord.

The experimental setup for testing the NACA4421 modified aerofoil is shown in Fig. 12(a). The slider mechanism and the polyurethane strip details are shown in Fig. 12(b). The trailing edge displacement of the aerofoil is measured using a laser displacement sensor. The temperature of the SMA wire is monitored using a thermocouple. The details of the experimental procedure are same as that for the NACA0012 aerofoil. The schematic diagram of the experimental setup is shown in Fig. 4. The variation in the applied voltage across the SMA wire is shown in Fig 6(a). Variation in the trailing edge deflection due to the change in SMA wire temperature is observed over a number of cycles of loading. Fig. 13 shows the variation in trailing edge displacement from 1st cycle to 200 cycles. From Fig. 13, it is seen that the trailing edge deflection of the aerofoil is initially about 3.3mm, which is consistent with the solution obtained, see Fig. 10. It is also observed from Fig. 13 that the trailing edge deflection decreases to about 2.8mm for 200th cycle and the hysteresis loop widens as the number of cycles progresses. These aspects are attributed to the degradation of the functional properties of the SMA wire. The multiple cycles of training on the SMA wire are done with the intension of studying this SMA wire degradation and its effects on the trailing edge deflection. These design analysis would be used to further refine and optimize the morphing mechanism.

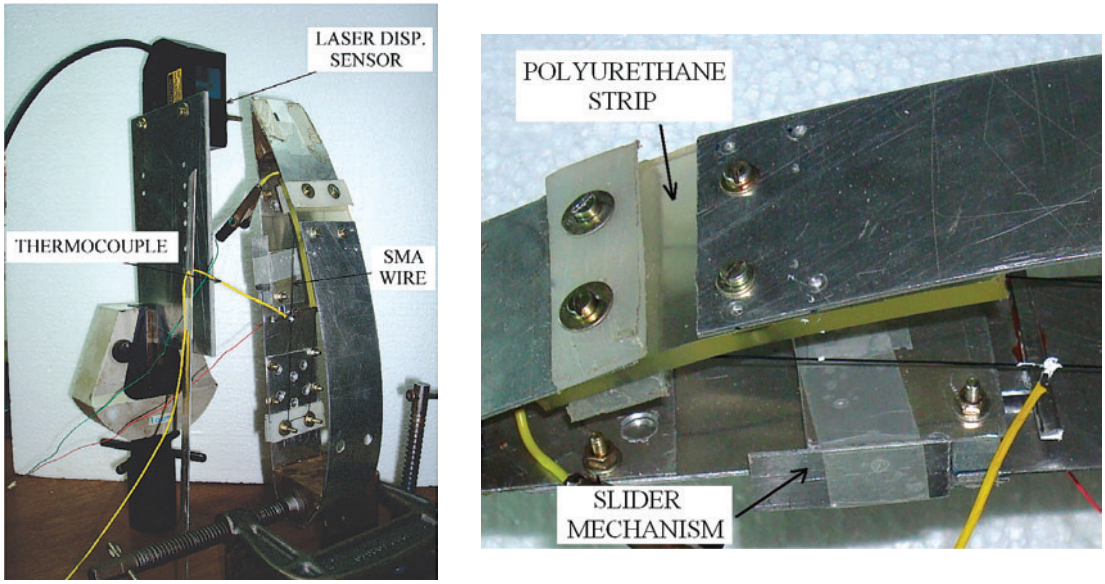

(a) (b)

Figure 12. (a) Experimental Setup of NACA4421 aerofoil (b) close-up of the polyurethane strip and the slider mechanism.

Usually, the SMA wires are stabilized under some constant pre-stress. The main problem in the present application is that, during thermal actuation, the stress varies widely. Therefore, the standard approach of first stabilizing the actuator under constant stress and then placing in the aerofoil is not valid. The actuators here should be (i) either stabilized under in-situ condition (ii) or stabilized first

under exact loading conditions and then placed in the aerofoil. The first method was chosen. Obviously, the second method is extremely complicated to realize, since the aerofoil stiffness varies as nonlinear function of actuator force. A rigorous optimization need to be done before applying such external stabilization process.

One of the important issues while using the SMA wire for aerofoil morphing is ensuring proper pre-stress in the SMA wire. Maximum deflection of the SMA wire would be obtained if the SMA wire is heated from the martensite state. In order to ensure that the SMA wire reaches a complete martensite state, a pre-stress higher than the critical transformation stress is required. Most importantly, here we are dealing with a thermal actuation under varying stress. Therefore, some stress (higher than the critical stress) needs to be maintained. In a strict sense, this critical transformation stress may not be always same as the transformation stress for superelastic transformation. If the SMA wire is not completely in martensite state, then SMA wire performance would not be optimum. Therefore, further studies are aimed at optimizing the SMA wire integrated aerofoil performance.

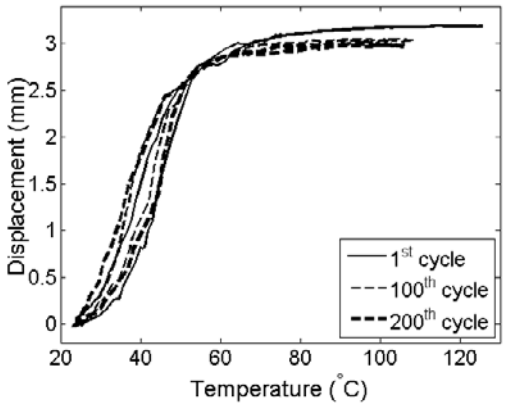

Figure 13. Trailing edge displacement for change in SMA wire temperature.

4. CONCLUSION

A finite element model of the SMA wire integrated aerofoil has been developed. This model also incorporates the aerodynamic loads on the aerofoil. The pressure distribution on the aerofoil is computed using a two-dimensional source-vortex panel code. This finite element model was used for preliminary analysis of NACA0012 aerofoil. Both stress-induced and temperature-induced actuation methods for SMA wire were analyzed. The stress-induced actuation of the SMA wire was found to be somewhat impractical due to high actuation stress requirements and weight constraints for the auxiliary actuation. Therefore temperature-induced actuation of the SMA wire has been used in both simulation and experimental implementation. The analysis of the NACA0012 and NACA4421 airfoils established the need for a mechanism to enhance the trailing edge deflection. Therefore a slider mechanism was conceived and it was attached on the lower skin of the NACA4421 aerofoil. The flexural stiffness of the upper skin was relaxed using a strip of polyurethane at 70% chord length. This re-designed aerofoil was tested for three different locations of the slider mechanism using a coupled multiphysics model. Based on the analysis, the location of the slider at 65% chord was found to be the optimal. Based on these results, a NACA4421 redesigned aerofoil was fabricated. Experimental results on this NACA4421 aerofoil agrees with the simulated result. Using this experimental setup, the SMA wire behavior and its degradation are being investigated to further refine the design towards UAV application.

ACKNOWLEDGEMENTS

Financial support from Aeronautical Development Agency (ADA), Bangalore, is thankfully acknowledged. We also thank Dr. S. Bhaumik of National Aerospace Laboratories (NAL), Bangalore, for providing the SMA wires.

REFERENCES

1. Bowman, J., et al., Development of Next Generation Morphing Aircraft Structures, *48th AIAA/ASME/ASCE/AHS/ASC Structures, Structural Dynamics, and Materials Conference*, Paper No. 1730, Honolulu, Hawaii, 2007.
2. Cesnik, C.E., Last, H.R., Martin, C.A., A Framework For Morphing Capability Assessment, *45th AIAA/ASME/ASCE/AHS/ASC Structures, Structural Dynamics and Materials Conference*, Paper No. 1654, Palm Springs, California, 2004.
3. Rodriguez, A.R., Morphing Aircraft Technology Survey, *45th AIAA Aerospace Sciences Meeting and Exhibit*, Paper No. 1258, Reno, Nevada, 2007.
4. Joslin, R.D., Jones, G.S., Applications of Circulation Control Technology, *Progress in Astronautics and Aeronautics*, Vol. 214, AIAA, 2006.
5. Trease, B.P., Kota, S., Synthesis of Adaptive and Controllable Compliant Systems with Embedded Actuators and Sensors, *ASME 2006 International Design Engineering Technical Conference and Computers and Information in Engineering Conference*, Paper No. 99266, Pennsylvania, 2006.
6. Amprikidis, M., Cooper, J.E., Sensburg, O., Experimental investigation of an all movable vertical tail model, *44th AIAA/ASME/ASCE/AHS/ASC Structures, Structural Dynamics, and Materials Conference*, Paper No. 1413, Norfolk, Virginia, 2003.
7. Ramrkahyani, D.S., Lesieutre, G.A., Frecker, M., Bharti, S., Aircraft Structural Morphing using Tendon Actuated Compliant Cellular Trusses, *45th AIAA/ASME/ASCE/AHS/ASC Structures, Structural Dynamics and Materials Conference*, Paper No. 1728, Palm Springs, California, 2004.
8. Perkins, D.A., Reed, J.L. Jr., Havens, E., Morphing Wing Structures for Loitering Air Vehicles, *45th AIAA/ASME/ASCE/AHS/ASC Structures, Structural Dynamics and Materials Conference*, Paper No. 1888, Palm Springs, California, 2004.
9. Cadogan, D., Smith, T., Uhelsky, F., Mackusick, M., Morphing inflatable wing development for compact package unmanned aerial vehicles, *AIAA SDM Adaptive Structures Forum*, Paper No. 1807, 2004.
10. Vos, R., Barrett, R., Breuker, R. D., Tiso, P., Post-buckled precompressed elements: a new class of control actuators for morphing wing UAVs, *Smart Materials and Structures*, Vol. 16, pp. 919-926, 2007.
11. Dong Yu, Boming Zhang, Lanin Jun, A changeable aerofoil actuated by shape memory alloy springs, *Materials Science and Engineering A*, Vol. No. 485, pp. 243-250, 2008
12. Strelec, J.K., Lagoudas, D.C., Khan, M.A., Yen, J., Design and Implementation of a Shape Memory Alloy Actuated Reconfigurable Airfoil, *Journal of Intelligent Material Systems and Structures*, Vol. 14, 2003.
13. Brinson, L.C., One dimensional constitutive behavior of shape memory alloys: thermomechanical derivation with non-constant material functions and redefined martensite internal variable, *Journal of Intelligent Materials Systems and Structures*, Vol. No. 4(2), pp. 229-242, 1993.